

Original Research Article

Total flavonoids of *Rhizoma drynariae* influence ferroptosis in osteoblasts via miR-205-5p/GPX4 axis

Enjun Kong¹, Yan Xu², Haichen Yang^{3*}

¹Department of Emergency, ²Department of Rheumatic Hematology, The People's Hospital of Danyang and Affiliated Danyang Hospital of Nantong University, Danyang 212300, ³Department of Emergency, Huai'an Hospital Affiliated of Xuzhou Medical University and Huai'an Second People's Hospital, Huai'an 223002, China

*For correspondence: **Email:** yhc7873890462021@163.com

Sent for review: 18 May 2022

Revised accepted: 22 June 2023

Abstract

Purpose: This research investigated the biological effects of total flavonoids of *Rhizoma Drynariae* (TFRD) on osteoporosis in mice.

Methods: Mice were subjected to bilateral ovariectomy (OVX) to generate the osteoporosis model used, which was then intragastrically administered TFRD daily at a dose of 75 mg/kg. Bone loss was examined histologically using H&E staining. Moreover, erastin-treated primary osteoblasts were used to further analyze the effect of TFRD on ferroptosis. Reactive oxygen species (ROS), ferrous iron level, and CCK-8 method were employed to determine the protective influence of TFRD against ferroptosis in erastin-treated osteoblasts. The relationship between microRNA-205-5p (miR-205-5p) and glutathione peroxidase 4 (GPX4) was determined using luciferase assay.

Results: TFRD treatment inhibited OVX-induced bone mass loss, downregulated ferrous ion content, and increased the level of GPX4 in vivo ($p < 0.01$). Besides, TFRD treatment inhibited erastin-induced increases in ROS level and ferrous iron level, and promoted cell viability in vitro ($p < 0.01$). Moreover, TFRD increased GPX4 protein expression level ($p < 0.01$). Results from gain and loss experiments showed that GPX4 increased cell viability, and reduced ferrous ion and ROS levels in erastin-induced osteoblasts ($p < 0.01$, $p < 0.001$, respectively). Furthermore, miR-205-5p directly targeted GPX4 and negatively regulated GPX4 expression ($p < 0.01$, $p < 0.001$, respectively). Upregulation of GPX4 reversed the effect of miR-205-5p overexpression on cell viability, and reduced ferrous iron level and ROS levels in osteoblasts significantly.

Conclusion: TFRD may serve as an inhibitor of osteoblast ferroptosis during osteoporosis formation by down-regulating the expression of miR-205-5p which directly targets GPX4 in mouse osteoblasts. These findings indicate the therapeutic potential and underlying mechanism of action of TFRD.

Keywords: Flavonoids, *Rhizoma drynariae*, MiR-205-5p GPX4, Ferroptosis, Osteoblasts

This is an Open Access article that uses a funding model which does not charge readers or their institutions for access and distributed under the terms of the Creative Commons Attribution License (<http://creativecommons.org/licenses/by/4.0>) and the Budapest Open Access Initiative (<http://www.budapestopenaccessinitiative.org/read>), which permit unrestricted use, distribution, and reproduction in any medium, provided the original work is properly credited.

Tropical Journal of Pharmaceutical Research is indexed by Science Citation Index (SciSearch), Scopus, Web of Science, Chemical Abstracts, Embase, Index Copernicus, EBSCO, African Index Medicus, JournalSeek, Journal Citation Reports/Science Edition, Directory of Open Access Journals (DOAJ), African Journal Online, Bioline International, Open-J-Gate and Pharmacy Abstracts

INTRODUCTION

Osteoporosis has become a major public health problem, and it is characterized by reduced bone

mass, damaged bone microstructure, and increased bone brittleness [1]. It not only impairs quality of daily living and mortality of the affected individuals, but also increases economic burden

on patients, families, and society. The miRNAs, which do not code for proteins, comprise small molecules 21-24 nucleotides long, which function in posttranscriptional regulation of gene expression. It has been proven that miRNAs form an indispensable part of the ferroptosis regulatory network by affecting ferroptosis-related physiological and pathological conditions [2,3]. Besides, ferroptosis-induced cell death usually exhibits unique cell morphology that is distinct when compared to other known cellular death pathways, e.g., abnormal mitochondrial morphology, cell membrane rupture, and cell disintegration [4-6].

The suppression of bone resorption is an ideal strategy for preventing osteoporosis. However, the adverse effects of this strategy limit its progress [7]. In recent years, more and more natural products have been used to treat osteoporosis. *Rhizoma drynariae* (RD) is currently a common agent for the treatment of osteoporosis. A previous study reported that the extracts of RD exerted a stimulatory effect on osteoblast proliferation and differentiation. The present study investigated the influence of TFRD on ferroptosis of osteoporosis, and the involvement of the miR - 205 - 5p/GPX4 axis in the process, in order to provide new therapeutic strategies for osteoporosis.

EXPERIMENTAL

Preparation of TFRD

Total flavonoids of *Rhizoma Drynariae* were obtained from Beijing Qihuang Pharmaceutical Manufacturing Co. Ltd (National Medicine permit no. Z20030007, product no. 04080081, DRTF content \geq 80 %).

Animals and treatment

Female C57Bl/6Hsd mice aged 6 - 8 weeks and weighing 18 - 20 g, were supplied by Animal Center of Nanjing University (Nanjing, China). The mice were kept in plastic cages in 12-h light/12-h dark cycle at 24 °C, and were allowed unrestricted access to feed and water. The mice were randomly assigned to 3 groups: sham (n = 5), ovariectomy (OVX; n = 5), and OVX + TFRD (n = 5) groups. To generate osteoporosis model, the mice were subjected to bilateral OVX as described in previous studies [8,9]. Mice from the sham group underwent bilateral laparotomy. Then, the mice were allowed to recover and maintained using standard feed and filtered water. Seven days after surgery, the ovariectomized mice were intragastrically administered TRFD daily at a dose of 75 mg/kg

(OVX + TFRD group) or 200 μ L phosphate buffered saline (PBS; OVX group) for one week. Thereafter, the mice were subjected to anesthesia using sodium pentobarbital (70 mg/kg). Then, blood was collected from the heart and long bones (femurs and tibias) for use in subsequent studies. All animal experiments received approval from the ethical authority of our institution (approval no. 20220402). The experiments were conducted in accordance with ARRIVE guidelines [10].

H&E staining

The femurs and tibias were fixed in 10 % formalin, followed by paraffin embedding, sectioning into 5- μ m-thick slices, and staining with H&E. The stained sections were subjected to light microscopic examination.

Iron assay

Intracellular ferrous iron (Fe^{2+}) level was assessed with Fe^{2+} assay kit (Sigma, USA) in line with the kit protocols.

Cell culture and treatment

The HEK 293T cells were obtained from ATCC (USA) and cultured in DMEM with 10 % fetal bovine serum (FBS). As described in a previous study [11], the osteoblasts were isolated from the calvaria tissue of newborn mice. In brief, following mice sacrifice, calvariae of the newborn mice were removed, cut and digested with collagenase A solution for 20, 50 and 90 min at 37 °C. The cells from the first digest were plated in a 10 - cm dish and cultured to 70 % confluency, followed by culturing in osteogenic medium with 10 mM β -glycerophosphate. After one week, the cells were used for further studies.

Erastin solution was purchased from Selleck Chemicals (Houston, USA). To generate ferroptosis model, osteoblasts were plated into 3-cm dish (10^5 cells per dish) and exposed to 5 μ M erastin for 24 h. Then, the cells were treated with 12.5 μ g/mL TFRD for 24 h. Control cells received solvent only.

Cell proliferation assay

Cell viability was evaluated using cell counting kit-8 (CCK - 8) (Sigma, USA) assay. Briefly, following various treatments, the osteoblasts were plated in 96-well plates (5000 cells/well) for 24 h, followed by addition of CCK-8 solution, and further incubation for 4 h. Then, the absorbance of each well was read at 450 nm in a microplate reader.

Western blot assay

Total protein was extracted from the cells after various treatments using RIPA buffer. The proteins were resolved with SDS-polyacrylamide gel electrophoresis. Subsequent electro-transfer onto PVDF filters was followed by blocking using 5 % BSA solution. Next, each membrane was subjected to overnight incubation with 1° immunoglobulins against GPX4 (ab125066, 1:2000) and GAPDH (ab8245, 1:5000) at 4 °C. Then, membrane incubation with related secondary antibodies (1:5000, Abcam, USA) for 2 h was done at room temperature. Glyceraldehyde-3-phosphate dehydrogenase (GAPDH) was used as the internal control. Finally, protein bands were determined using ECL kit, while quantification was done with Image J software.

Immunofluorescence (IF) staining

Osteoblasts were fixed with 4 % paraformaldehyde for 15 min, and permeabilized with 0.2 % Triton X-100. Next, the cells were blocked with 5 % bovine serum albumin for 2 h at room temperature, followed by overnight incubation with antibody against GPX4 (cat no. ab125066, 1 µg/mL, Abcam, USA) at 4 °C, and subsequently with Alexa Fluor-647-conjugated secondary antibody (cat no. ab150083, Abcam, USA) for 2 h at room temperature. The nuclei were stained with 4', 6-diamidino-2-phenylindole dihydrochloride (DAPI; Thermo, USA). The stained cells were photographed under fluorescence microscopy.

Evaluation of reactive oxygen species (ROS)

Osteoblasts were plated into a 3-cm dish at a density of 10⁶ cells/dish and maintained in a serum-free medium. Then, 10 µM 2', 7'-dichlorodihydrofluorescein diacetate (DCFH-DA, MedChemExpress, China) was added to the cells and left for 30 min. The cells were imaged using a fluorescence microscope.

Cell transfection

The mmu-miR-205-5p mimic and related control (mimic-NC) were obtained from RiboBio

(Guangzhou, China). The GPX4 overexpressed vector (GPX4 - OE), knockdown vector (GPX4 - KD) and blank vector were products of GemmaPharma, China. The cells were seeded in 3-cm dish at a density of 10⁶ cells/dish. Then, 20 µM miR-205-5p mimic or 5 µg plasmid was transfected into the cells with Lipofectamine 3000 kit (Invitrogen, USA), in line with the manufacturer's instructions.

Quantitative reverse transcription polymerase chain reaction (qRT-PCR)

Cells were collected after different treatments, and TRIzol (Thermo, USA) was used for extraction of total RNA. Then, RNA from each sample was reverse-transcribed into cDNA using the PrimeScript miRNA cDNA Synthesis Kit (TaKaRa, Japan). The expression levels of miRNAs were determined on the qRT-PCR system (Bio - Rad, USA) in line with the manufacturer's protocol. Finally, relative mRNA levels were calculated using the 2^{-ΔΔCT} method and normalized to the expression level of U6. Table 1 shows the primers used.

Luciferase assay

The 3'UTR of wildtype GPX4 (GPX4-WT) with interaction sites for miR-205-5p was cloned into the pmirGLO vector (Promega, USA). The 3'UTR of mutant GPX4 (GPX4-MUT) was established using site-specific mutagenesis kit. Using Lipofectamine 3000, the human embryonic kidney 293T (HEK293T) cells were co-transfected with GPX4 - WT, GPX4 - MUT, miR-205-5p mimic, miR-205-5p blocker or associated control for 48 h. Then, luciferase level was determined with the dual-luciferase reporter assay method (Promega, USA). The data were normalized using renilla luciferase.

Statistics

Statistical analysis was done with GraphPad Prism 8.0 software. Data are shown as mean ± SD (n = 3). Two-group comparison was done with *t*-test, while ANOVA and Duncan's post-hoc tests were used for multi-group comparison. Statistical significance was assumed at *p* < 0.05.

Table 1: Primers employed for qRT-PCR

Gene	Forward Primer (5' - 3')	Reverse Primer (5' - 3')
miR-214-5p	CGCGATGCCTGTCTACACTTG	AGTGCAGGGTCCGAGGTATT
miR-205-5p	CGTCCTTCATTCCACCGG	AGTGCAGGGTCCGAGGTATT
U6	GCTTCGGCAGCACATATACTAAAAT	CGCTTCAGAAATTTGCGTGTTCAT

RESULTS

TFRD alleviated iron-induced osteoblast cell death

A bilateral ovariectomy (OVX) mouse model was established for investigation of the effect of TFRD on osteoporosis. As shown in Figure 1 A, a complete and orderly-arranged bone trabeculae structure was seen in sham group. Tissues from OVX group exhibited loose bone trabeculae. However, TFRD treatment inhibited OVX-induced bone mass loss. To test the involvement of ferroptosis in the tibia bone tissue in osteoporosis *in vivo*, the ferrous iron content was determined, and results showed that ferrous iron level was increased in the OVX model (Figure 1 B). The protein level of GPX4, a key inhibitor of ferroptosis, was also decreased (Figure 1 C), implying that ferroptosis was induced in the bone tissue in the OVX model. In contrast, the TFRD treatment significantly downregulated the ferrous iron content caused by OVX surgery, and increased the level of GPX4, implying that TFRD prevented ferroptosis in the OVX-induced osteoporosis model (Figures 1 B and C).

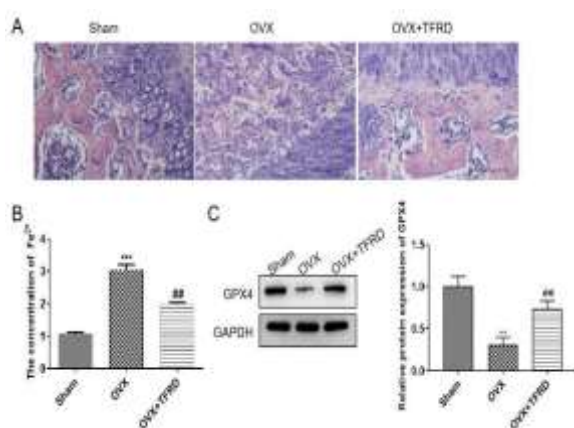


Figure 1: TFRD alleviated osteoporosis, suppressed ferrous iron level, and increased GPX4 level. A: H&E images of long bone (scale = 200 μ m). B: Concentrations of ferrous iron in tibia tissues. C: Levels of GPX4 in tibia tissues; the bands were statistically analyzed using Image J. Data are shown as mean \pm SD (n = 3). * P < 0.05, ** < 0.01, *** < 0.001, vs. sham group; # p < 0.05, ## < 0.01, ### < 0.001, vs. OVX group

To further study the role of TFRD in the ferroptosis in osteoblasts, an *in vitro* model of the erastin-treated primary osteoblasts was established. Erastin exhibited significantly increased ROS level and ferrous iron level, and suppressed cell viability, when compared to the control group, but these effects were reversed with the TFRD treatment (Figure 2 A - C), indicating that TFRD prevented ferroptosis in osteoblasts.

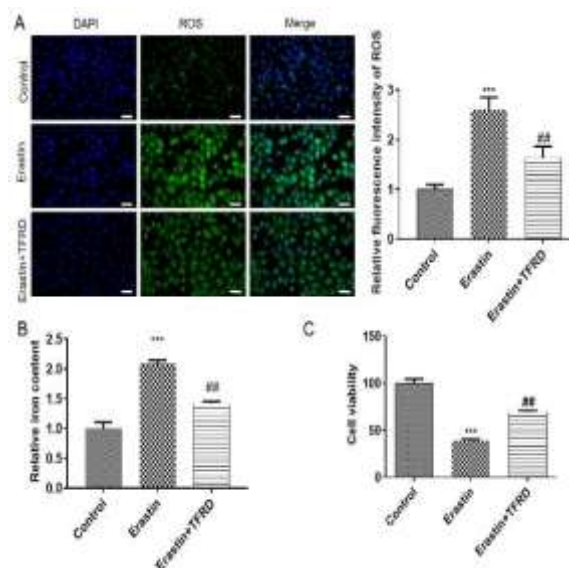


Figure 2: TFRD inhibited osteoblast ferroptosis. A: Fluorescence images of ROS in the osteoblasts. B: Concentration of iron in the osteoblasts. C: Cell viability of osteoblasts. Results are shown as mean \pm SD (n = 3). * P < 0.05, * p < 0.01, ** p < 0.001 vs. control; # p < 0.05, ## p < 0.01, ### p < 0.001 vs. erastin group

TFRD inhibited osteoblast ferroptosis by regulating GPX4

As shown in Figure 3 A and B, erastin suppressed the protein level of GPX4, whereas co-treatment with erastin and TFRD increased GPX4 protein expression level. The gain and loss experiments showed that GPX4 expression was about two folds higher in the erastin + GPX4 - OE group, when compared with erastin + vector 1 group (Figure 3 C and D). Conversely, the erastin + TFRD + GPX4 - KD group had significantly downregulated GPX4 expression, when compared with the erastin + vector 2 + TFRD group (Figure 3 C and D).

Overexpression of GPX4 increased cell viability, and reduced ferrous iron level and ROS level in erastin-treated osteoblasts (Figure 4 A - C). However, TFRD and overexpression of GPX4 had similar effects on cell viability, ferrous iron level and ROS level in erastin-treated osteoblasts (Figure 4 A - C). Besides, the knockdown of GPX4 suppressed cell viability, and increased ferrous iron level and ROS level in erastin and TFRD-treated osteoblasts (Figure 4 A - C). These data suggest that TFRD-mediated osteoblast ferroptosis was GPX4-dependent.

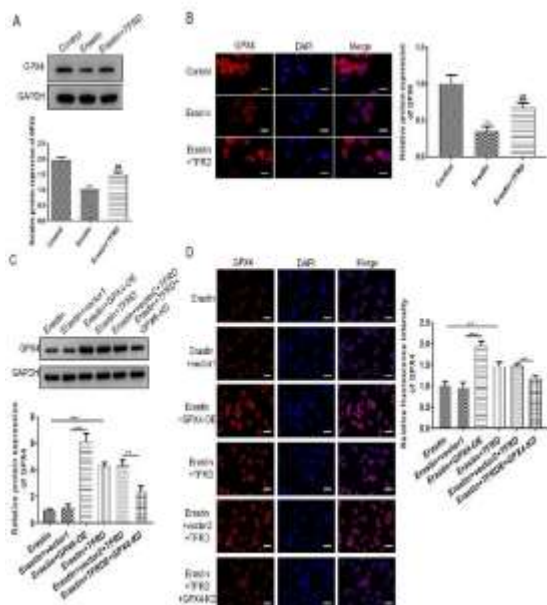


Figure 3: TFRD inhibited osteoblast ferroptosis via regulation of GPX4 expression. A: Protein levels of GPX4 in osteoblasts. B: Immunofluorescence images of the expression of GPX4 in the osteoblasts (scale = 20 μ m). C and D: Expressions of GPX4 (scale = 20 μ m). All results are shown as mean \pm SD (n = 3). *** P < 0.001 vs. control group, ### p < 0.01, vs. erastin

miRNAs for GPX4 were predicted using miRWalk, miRanda, RNA22, targetscan, RNAhybrid, and miRMA. The eight overlapped miRNAs were selected for further analysis. Based on the criteria of prevalent miRNAs in mice, and homologs in humans, two miRNAs, i.e., mmu-miR-214-3p and mmu-miR-205-5p were chosen for qRT-PCR assay (Figure 5 A). The results showed that TFRD decreased miR-205-5p expression (Figure 5 B). Moreover, TFRD decreased miR-205-5p expression time- and dose-dependently (Figures 5 C and D), while TFRD increased GPX4 protein expression time- and dose-dependently (Figures 5 E and F). Luciferase assay results showed that luciferase activity was significantly attenuated in cells with co-transfection, wild type GPX4 3'UTR and the miR-205-5p mimetic, but was enhanced in cells with co-transfection with wild type GPX4 3'UTR and the miR-205-5p inhibitor. Conversely, miR-205-5p mimic transfection had no effect on the vector containing the mutant one (Figure 5 G and H). Next, the study investigated the effect of miR-205-5p on the protein level of GPX4 in osteoblasts. As shown in Figure 5 I, osteoblasts transfected with the miR-205-5p mimic showed a 60 % reduction in the protein level of GPX4, when compared with mimic-NC group, whereas those transfected with the miR-205-5p inhibitor showed a significant increase in GPX4, when compared to the related NC group. These data suggest that miR-205-5p directly targeted GPX4 in osteoblasts.

MiR-205-5p regulated ferroptosis in osteoblasts via GPX4

To assess the involvement of miR-205-5p/GPX4 axis in ferroptosis in osteoblasts, osteoblasts were treated with erastin and transfected with miR-205-5p mimic and GPX4 overexpression vector. Successful transfection of the miR-205-5p mimic was verified using qRT-PCR (Figure 6 A). Moreover, in cells treated with erastin, the GPX4 expression increased significantly for cells co-transfected with vectors overexpressing GPX4 and mimic NC, and decreased in cells co-transfected with miR-205-5p and empty vector1 (Figure 6 B). The co-transfection of miR-205-5p suppressed the effect of GPX4-OE on GPX4 protein expression level (Figure 6 B). Consistently, immunofluorescence assay presented the highest positive signal of GPX4 in the GPX4-overexpressed groups, and the lowest in the miR-205-5p group. However, the elevated positive signal of GPX4 induced by the transfection of the vector overexpressing GPX4 was blocked by the co-transfection of miR-205-5p (Figure 6 C).

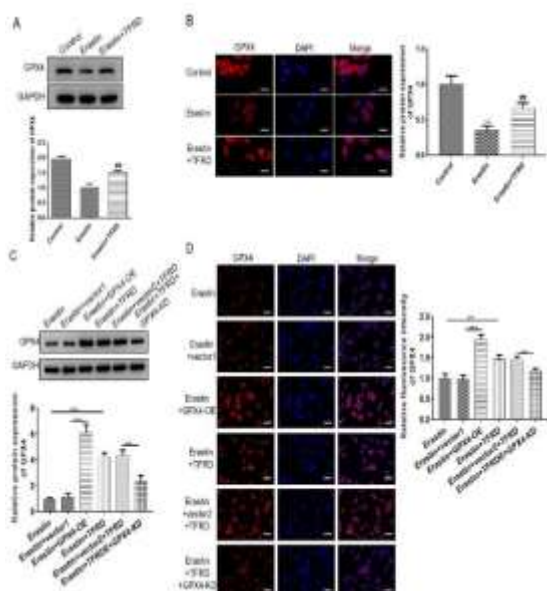


Figure 4: A: Cell viability of osteoblasts. B: Concentrations of ferrous iron in the osteoblasts. C: Fluorescence images of ROS in osteoblasts (scale = 20 μ m). Data are shown as mean \pm SD. * P < 0.05, ** < 0.01, *** < 0.001, vs. erastin group or erastin + vector 1 group, or erastin + vector 2 + TFRD group

MiR-205-5p targeted GPX4 in TFRD-treated osteoblasts

To further explore the mechanism underlying the role of GPX4 in osteoblasts, the potential

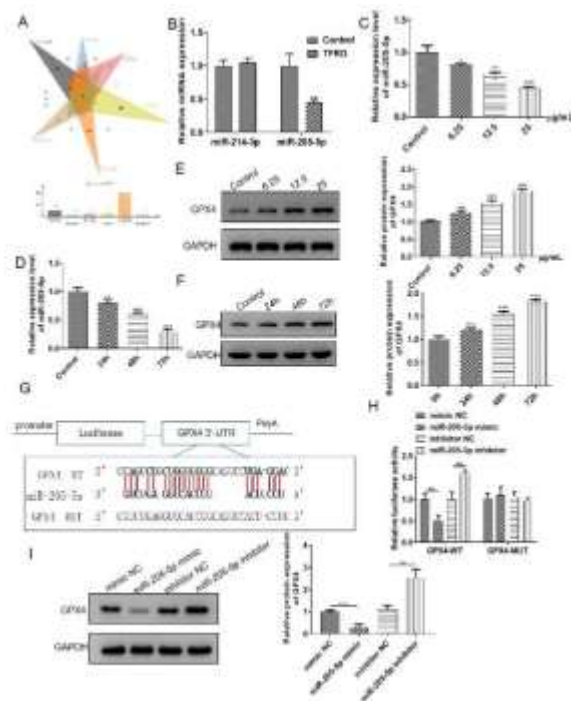


Figure 5: MiR-205-5p regulated the effect of TFRD in osteoblasts. A: Bioinformatical analysis was used to predict the potential targeted miRNAs for GPX4. B: Expression profiles of miR-214-3p and miR-205-5p in the control cells and TFRD-treated cells. C: Osteoblasts were treated with TFRD for 24 h at 3 graded doses, and the level of miR-205-5p was analyzed. D: Cells were incubated with TFRD at a dose of 12.5 $\mu\text{g}/\text{mL}$, and miR-205-5p was determined at 24 h, 48 h and 72 h. E: GPX4 protein levels in osteoblasts after TFRD treatment for 24 h at 3 graded doses. F: Protein level of GPX4 in osteoblasts after TFRD treatment at 24 h, 48 h and 72 h. G: Binding sites between GPX4 3'UTR and miR-205-5p. H: Luciferase assay was used to detect the relationship between GPX4 and miR-205-5p. I: miR-205-5p negatively regulated GPX4 expression. Results are expressed as mean \pm SD (n = 3). * $P < 0.05$, ** $p < 0.01$, *** $p < 0.001$, vs. control or mimic NC group or inhibitor NC group

Subsequent analysis showed that elevated miR-205-5p decreased cell viability, increased ferrous iron level and ROS level, and reversed the protective function of overexpressed GPX4 in osteoblasts treated with erastin (Figure 7 A - C). Collectively, these findings indicate that miR-205-5p acted as the mediator of ferroptosis in osteoblasts via GPX4.

DISCUSSION

After menopause, fluctuating hormonal levels increase the risk of many diseases such as cardiovascular disease and osteoporosis. In addition, every year, loss of ovarian function and premature menopause induced by oophorectomy,

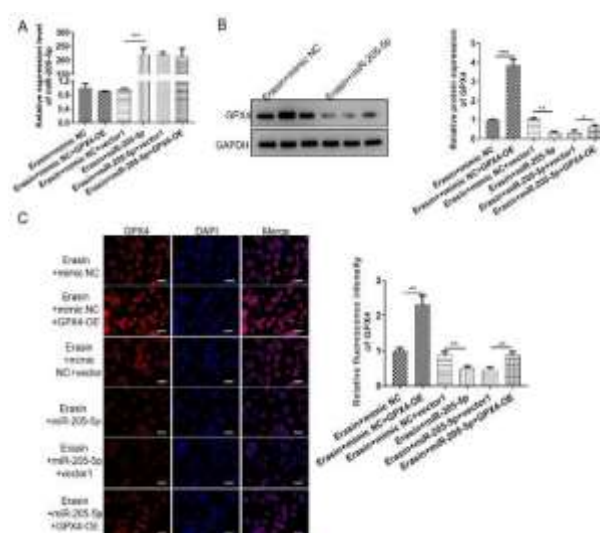


Figure 6: MiR-205-5p regulated ferroptosis via GPX4. A: Transfection efficiency of miR-205-5p. B: Blots for the protein levels of GPX4 in osteoblasts after GPX4-OE or miR-205-5p mimic transfection prior to erastin administration. C: Immunofluorescence images of the expressions of GPX4 in osteoblasts with different treatments (scale = 20 μm). Data are shown as mean \pm SD (n = 3). * $P < 0.05$, ** < 0.01 , *** < 0.001 , vs. Erastin + mimic NC group or erastin + mimic NC + vector 1 group or erastin + miR-205-5p + vector 1 group

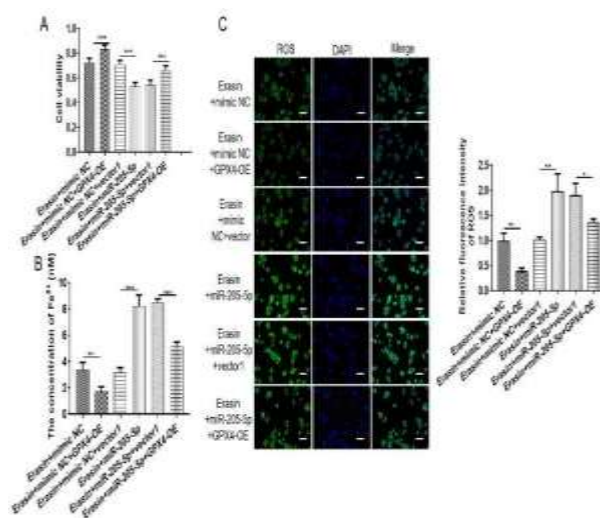


Figure 7: MiR-205-5p regulated ferroptosis via GPX4. A: Cell viability of osteoblasts. B: Concentration of ferrous iron in the osteoblasts. C: Fluorescence images of ROS in osteoblasts after different treatments (scale = 20 μm). Data are shown as mean \pm SD (n = 3). * $P < 0.05$, ** < 0.01 , *** < 0.001 vs. Erastin + mimic NC group or erastin + mimic NC + vector 1 group, or erastin + miR-205-5p + vector 1 group

radiotherapy, and chemotherapy due to various gynecological cancer operations pose threaten to women under the age of 45 years [12,13].

Osteoporosis is a common cause of low back pain, kyphosis, and sciatica in menopausal women, thereby affecting their quality of life.

Iron metabolism participates in bone growth and formation. Recently, a newly defined type of programmed cell death, ferroptosis, has been widely implicated in diseases and metabolism closely related to iron metabolism disorders. Different from apoptosis, autophagy, or necrosis, ferroptosis process is inhibited by GPX4 and System Xc⁻, leading to interruption of cysteine metabolism and enhanced lipid peroxidation [14-16]. The disordered reoxidation status results in the accumulation of ROS, leading to the disruption of the cell membrane [17,18]. The relationship between the abnormal expression of GPX4 and the oxidative stress of osteoblasts and osteoclasts suggests that iron apoptosis may be involved in bone disorders.

The present study showed that in OVX model, the levels of ROS and Fe²⁺ were increased in the bone tissue, whereas the GPX4 protein level was decreased, implying a stimulation of ferroptosis in the osteoporosis model. In addition, the supplementation with TFRD decreased the ROS and Fe²⁺ levels, and enhanced the GPX4 protein level, indicating that the TFRD alleviated ferroptosis in bone tissue caused by the osteoporosis. Consistently, erastin-induced ferroptosis in mice primary osteoblasts was also alleviated by TFRD via increases in GPX4 protein level and decreases in the levels of ROS and Fe²⁺.

It has been reported that miRNAs play important regulatory roles in various diseases, and several miRNAs have been shown to serve as positive or negative regulators of osteoblast differentiation and bone formation [19-22]. In this study, through bioinformatical analysis and luciferase studies, it was found that miR-205-5p directly targeted GPX4. The MiR-205-5p has been implicated in some diseases [23,24]. For instance, miR-205-5p activated ERK/AKT pathway by targeting ANGPT2, thereby inhibiting human endometriosis progression in endometrial stromal cells [23].

In addition, miR-205-5p/FOXO1 axis promoted progression of endometrial cancer under paclitaxel treatment [24]. After treatment with TFRD, a significant decline in miR-205-5p was observed in the *in vitro* model of osteoblast ferroptosis. Furthermore, it was found that miR-205-5p promoted ROS and Fe²⁺ levels in osteoblasts by targeting GPX4, thereby inducing ferroptosis.

CONCLUSION

The findings of this study indicate that TFRD may serve as an inhibitor of osteoblast ferroptosis during osteoporosis formation by down-regulating miR-205-5p which directly targets GPX4 in mouse osteoblasts. Thus, TFRD has potentials for development into a drug for the management of osteoporotic disorders.

DECLARATIONS

Acknowledgements

None provided.

Funding

None provided.

Ethical approval

None provided.

Availability of data and materials

The datasets used and/or analyzed during the current study are available from the corresponding author on reasonable request.

Conflict of Interest

No conflict of interest associated with this work.

Contribution of Authors

We declare that this work was done by the authors named in this article and all liabilities pertaining to claims relating to the content of this article will be borne by the authors. Enjun Kong and Haichen Yang conceived and designed the study, and drafted the manuscript while Enjun Kong, Yan Xu and Haichen Yang collected, analyzed and interpreted the experimental data. Enjun Kong and Yan Xu revised the manuscript for important intellectual content. All authors read and approved the final manuscript.

Open Access

This is an Open Access article that uses a funding model which does not charge readers or their institutions for access and distributed under the terms of the Creative Commons Attribution License (<http://creativecommons.org/licenses/by/4.0>) and the Budapest Open Access Initiative (<http://www.budapestopenaccessinitiative.org/read>), which permit unrestricted use, distribution,

and reproduction in any medium, provided the original work is properly credited.

REFERENCES

1. Toulis KA, Anastasilakis AD, Polyzos SA, Makras P. Targeting the osteoblast: approved and experimental anabolic agents for the treatment of osteoporosis. *Hormones (Athens)* 2011; 10: 174-195.
2. Bellavia D, Salamanna F, Raimondi L, De Luca A, Carina V, Costa V, Alessandro R, Fini M, Giavaresi G. Deregulated miRNAs in osteoporosis: effects in bone metastasis. *Cell Mol Life Sci* 2019; 76: 3723-3744.
3. Jin D, Wu X, Yu H, Jiang L, Zhou P, Yao X, Meng J, Wang L, Zhang M, Zhang Y. Systematic analysis of lncRNAs, mRNAs, circRNAs and miRNAs in patients with postmenopausal osteoporosis. *Am J Transl Res* 2018; 10: 1498-1510.
4. Dixon SJ, Stockwell BR. The hallmarks of ferroptosis. *Ann Rev Cancer Biol* 2019; 3: 35-54.
5. Yang Y. Regulation of ferroptosis by MicroRNAs. In: *Ferroptosis in Health and Disease*. Springer 2019; 125-145.
6. Phanichwong P, Apivatgaroon A, Boonsaeng WS. Prevalence of Os Acromiale in Thai Patients With Shoulder Problems: A Magnetic Resonance Imaging Study. *Orthop J Sports Med* 2022; 10: 23259671221078806.
7. Khosla S, Shane E. A crisis in the treatment of osteoporosis. In: *Wiley Online Library*, 2016.
8. Xiao L, Zhong M, Huang Y, Zhu J, Tang W, Li D, Shi J, Lu A, Yang H, Geng D et al. Puerarin alleviates osteoporosis in the ovariectomy-induced mice by suppressing osteoclastogenesis via inhibition of TRAF6/ROS-dependent MAPK/NF- κ B signaling pathways. *Aging* 2020; 12: 21706-21729.
9. Qi M, Zhang L, Ma Y, Shuai Y, Li L, Luo K, Liu W, Jin Y. Autophagy Maintains the Function of Bone Marrow Mesenchymal Stem Cells to Prevent Estrogen Deficiency-Induced Osteoporosis. *Theranostics* 2017; 7: 4498-4516.
10. Percie du Sert N, Hurst V, Ahluwalia A, Alam S, Avey MT, Baker M, Browne WJ, Clark A, Cuthill IC, Dirnagl U et al. The ARRIVE guidelines 2.0: Updated guidelines for reporting animal research. *J Cereb Blood Flow Metab* 2020; 40: 1769-1777.
11. Doolittle ML, Ackert-Bicknell CL, Jonason JH. Isolation and Culture of Neonatal Mouse Calvarial Osteoblasts. *Methods Mol Biol* 2021; 2230: 425-436.
12. Conrad M, Angeli JPF, Vandenabeele P, Stockwell BR. Regulated necrosis: disease relevance and therapeutic opportunities. *Nat Rev Drug Discov* 2016; 15: 348-366.
13. Hernandez C, Beaupre G, Carter D. A theoretical analysis of the relative influences of peak BMD, age-related bone loss and menopause on the development of osteoporosis. *Osteoporos Int* 2003; 14: 843-847.
14. Huang J, Chen G, Wang J, Liu S, Su J. Platycodin D regulates high glucose-induced ferroptosis of HK-2 cells through glutathione peroxidase 4 (GPX4). *Bioengineered* 2022; 13: 6627-6637.
15. Lee WC, Guntur AR, Long F, Rosen CJ. Energy Metabolism of the Osteoblast: Implications for Osteoporosis. *Endocr Rev* 2017; 38: 255-266.
16. Matsumoto H, Coccioni R, Frontalini F, Shirai K, Jovane L, Trindade R, Savian JF, Kuroda J. Mid-Cretaceous marine Os isotope evidence for heterogeneous cause of oceanic anoxic events. *Nat Commun* 2022; 13: 239.
17. Medeiros DM. Copper, iron, and selenium dietary deficiencies negatively impact skeletal integrity: A review. *Exp Biol Med* 2016; 241: 1316-1322.
18. Yin J, Han L, Cong W. Alpinumisoflavone rescues glucocorticoid-induced apoptosis of osteocytes via suppressing Nox2-dependent ROS generation. *Pharmacol Rep* 2018; 70: 270-276.
19. Kureel J, Dixit M, Tyagi A, Mansoori M, Srivastava K, Raghuvanshi A, Maurya R, Trivedi R, Goel A, Singh D. miR-542-3p suppresses osteoblast cell proliferation and differentiation, targets BMP-7 signaling and inhibits bone formation. *Cell Death Dis* 2014; 5: e1050-e1050.
20. Lu Z, Xu Y, Yao Y, Jiang S. miR-205-5p contributes to paclitaxel resistance and progression of endometrial cancer by downregulating FOXO1. *Oncol Res* 2019. PMID: 30982496.
21. Zhou CF, Liu MJ, Wang W, Wu S, Huang YX, Chen GB, Liu LM, Peng DX, Wang XF, Cai XZ, et al. miR-205-5p inhibits human endometriosis progression by targeting ANGPT2 in endometrial stromal cells. *Stem Cell Res Ther* 2019; 10: 287.
22. Ma S, Wang DD, Ma CY, Zhang YD. microRNA-96 promotes osteoblast differentiation and bone formation in ankylosing spondylitis mice through activating the Wnt signaling pathway by binding to SOST. *J Cell Biochem* 2019; 120: 15429-15442.